CHEMISTRY
A European Journal

Accepted Article

Authors: Venkata Suresh Mothika, Papri Sutar, Parul Verma, Shubhajit Das, Swapan K Pati, and Tapas Kumar Maji

WILEY-VCH

Regulating Charge-Transfer in Conjugated Microporous Polymer for Photocatalytic Hydrogen Evolution

Venkata Suresh Mothika[a],#, Papri Sutar[a],#, Parul Verma[a], Shubhajit Das[b], Swapan K Pati[b] and Tapas Kumar Maji[a],*

# These authors have contributed equally.

Abstract: Band gap engineering in donor-acceptor conjugated microporous polymers is a potential way to increase the solar energy harvesting towards photochemical water splitting. Herein, we report design and synthesis of a series of donor-acceptor CMPs [tetraphenylethylene (TPE) = donor and 9-fluorenone (F) = acceptor], **F$_{0.1}$CMP**, **F$_{0.5}$CMP** and **F$_{2.0}$CMP** which exhibit tunable band gaps and photocatalytic hydrogen evolution from water. The donor-acceptor CMPs exhibit intramolecular charge transfer (ICT) absorption in the visible region (λ_{max}=480 nm) and their band gap is finely tuned from 2.8 eV to 2.1 eV by increasing the 9-fluorenone content. Interestingly, they also show charge transfer emissions (in 540 -580 nm range), assisted by the energy transfer from the other TPE segments (not involved in CT interaction) as evidenced from fluorescence lifetime decay analysis. By increasing the 9-fluorenone content the emission color of the polymer is also tuned from green to red. Photocatalytic activities of the donor-acceptor CMPs (**F$_{0.1}$CMP**, **F$_{0.5}$CMP** and **F$_{2.0}$CMP**) are greatly enhanced compared to the 9-fluorenone free polymer (**F$_{0.0}$CMP**) which is essentially due to improved visible light absorption and low band gap of donor-acceptor CMPs. Among all the polymers **F$_{0.5}$CMP** with an optimum band gap (2.3 eV) shows highest H$_2$ evolution under visible light irradiation. Moreover, all the polymers show excellent dispersibility in organic solvents and also they are easily processed onto solid substrates.

Introduction

Conversion of solar energy into useful chemical energy as observed in nature is a source of inspiration for chemists to build artificial systems for mimicking its sophisticated working principle of water splitting.[1] Several inorganic, organic and inorganic-organic hybrid materials have been developed which convert solar energy to hydrogen fuel by water splitting.[2] Last decades have witnessed upsurge in the development of organic polymers as photocatalyst for hydrogen evolution.[3] Enormous efforts have been devoted for the improvement of their photocatalytic performance.[4] The most widely investigated organic polymers, such as graphitic C$_3$N$_4$, triazine-cored frameworks, hydrazone covalent organic frameworks and nitrogen containing covalent organic polymers often demand presence of platinum co-catalyst for H$_2$ evolution.[5] In addition, it is difficult to systematically tune the physicochemical properties of these polymers because of the limited synthetic routes and restricted structural diversity of the monomeric building blocks. In this regard, conjugated microporous polymers (CMPs) are superior as they have the wide synthetic diversity that allows selection of desired monomers.[6] Moreover, the permanent porosity of CMPs provides additional facilities for various practical applications.[7] In addition, when the building blocks are chromophoric monomers, the fine control over monomer stoichiometric compositions could lead to the formation of series of CMPs whose optical band gap could be systematically tuned. Recently, Cooper *et al.,* demonstrated statistical copolymerization as a tool to tune optical band gaps and studied photocatalytic H$_2$ evolution under visible light.[4c] Lowering of band gap allows capture of more visible photons for the generation of sufficient charge-carriers in the photo-excited state.[4a-c] Both the generation of charge-carriers and immediate migration to the catalyst surface are important in photocatalytic water splitting.[8] In general, organic materials have high exciton-binding energies due to low dielectric constants.[9] It was shown with linear polymers that integration of donor and acceptor moieties into a single organic material eases the exciton dissociation and charge-carriers generation.[10] Particularly, donor-acceptor polymers exhibiting ground state charge-transfer transition are more promising as the photo-excitation results in immediate charge separation.[11] Similar approach can also be implemented to develop donor-acceptor CMPs.[12] By changing the donor and acceptor ratio in the CMPs, the extend of charge and energy transfer can be modulated. This will widely tune the band gap and corresponding emission color of donor-acceptor CMPs. Implementation of this concept to design donor-acceptor CMPs to tune the band gap is unprecedented. In addition, easy visible-light excitation, sufficient charge-carrier generation and fast migration of charge-carriers in such donor-acceptor CMPs would be beneficial for efficient visible-light-driven water splitting for hydrogen evolution.
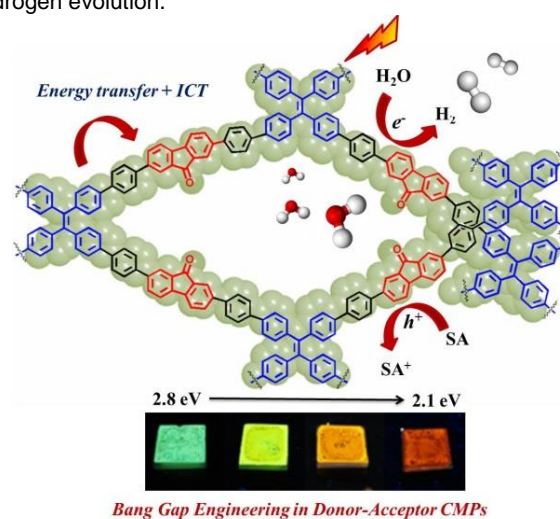
**Scheme 1.** Schematic representation of **F$_x$CMPs** showing energy transfer assisted intra-ligand charge transfer emission that tunes the band gap over a wide range and facilitate the photocatalytic H$_2$ evolution under visible light irradiation.

Herein, a series of donor-acceptor CMPs containing tetraphenylethene (TPE) as donor and varying concentration of 9-fluorenone as acceptor (**F$_{0.0}$CMP, F$_{0.1}$CMP, F$_{0.5}$CMP** and **F$_{2.0}$CMP)** are prepared (Scheme 1). 9-fluorenone is well known acceptor chromophore to show inter-ligand charge transfer transition when connected to a π-conjugated chromophore. A systematic increase of acceptor content (9-fluorenone = 0, 0.1, 0.5, 2.0 equivalent) indeed allowed us to regulate extent of charge-transfer in the **F$_x$CMP**. Concomitantly, the optical band gap decreases from 2.8 eV to 2.1 eV in **F$_{0.0}$CMP, F$_{0.1}$CMP, F$_{0.5}$CMP** and **F$_{2.0}$CMP**, respectively (Scheme 1). All the **F$_x$CMPs** show H$_2$ evolution (no co-catalyst added) under visible-light and broad-spectrum irradiation and they are highly recyclable. The **F$_{0.5}$CMP** with an optimum band gap (2.3 eV) shows H$_2$ evolution of 659.55 µmol g^{-1} h^{-1} under visible light (>420 nm) irradiation. While under broad irradiation (>290 nm), **F$_{0.5}$CMP** shows H$_2$ evolution of 1759.92 µmol g^{-1} h^{-1}.

Results and Discussion

Polymers **F$_{0.0}$CMP, F$_{0.1}$CMP, F$_{0.5}$CMP** and **F$_{2.0}$CMP** (the number indicates the equivalents of 2,7-Dibromo-9-fluorenone used for synthesis) are synthesized by Pd-catalyzed Suzuki-Miyura cross coupling reaction between tetrakis(4-bromophenyl)ethane (Figure S1), 2,7-dibromo-9-fluorenone and 1,4-benzene diboronic acid (Scheme 2). All the polymers are purified by Soxhlet extraction using tetrahydrofuran (THF) and methanol for 48 hours each. Fourier transform infrared spectroscopy (FT-IR) of **F$_{0.0}$CMP** shows bands at 1647 cm^{-1} and 3030 cm^{-1} corresponding to C=C of TPE and aromatic C-H stretching vibrations respectively (Figure S2). **F$_{0.1}$CMP, F$_{0.5}$CMP** and **F$_{2.0}$CMP** show strong bands at 1480 cm^{-1} corresponding to the aromatic C=C stretching vibrations of TPE and 9-fluorenone moieties. Moreover, C=O stretching frequency at 1712 cm^{-1} confirms the presence of 9-fluorenone in respective polymers. Formation of the **F$_x$CMPs** is further supported by solid-state ^{13}C-CP-MAS NMR spectroscopy (Figure S3, S4, S5 and S6). The strong signals in the range of 120-140 ppm are assigned to aromatic carbon atoms, whereas the moderate signal at 192 ppm is assigned to carbonyl carbon of **F$_x$CMPs**. As expected, **F$_{0.0}$CMP** did not show any signal for C=O in ^{13}C-CP-MAS NMR spectrum. Notably, the intensity of C=O signal enhances with
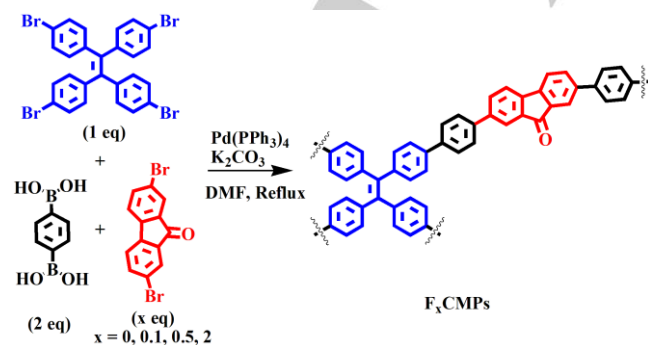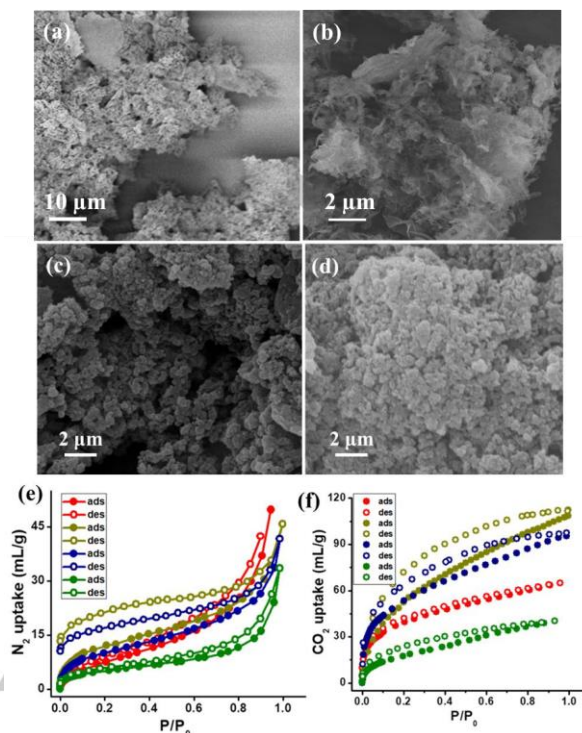

Figure 1. FESEM images (LEI mode) of a) **F$_{0.0}$CMP**, b) **F$_{0.1}$CMP**, c) **F$_{0.5}$CMP** and d) **F$_{2.0}$CMP**, e) N$_2$ adsorption isotherms at 77 K and f) CO$_2$ adsorption isotherms at 195 K of **F$_{0.0}$CMP** (red), **F$_{0.1}$CMP** (olive), **F$_{0.5}$CMP** (blue) and **F$_{2.0}$CMP** (green). The closed symbol indicates adsorption and open symbol indicates desorption.

increasing amount of 2,7-dibromo-9-fluorenone, used during the synthesis of **F$_{0.1}$CMP, F$_{0.5}$CMP** and **F$_{2.0}$CMP**. Powder X-ray diffraction (PXRD) patterns of **F$_x$CMPs** show broad peak around 2θ=20°, suggesting the amorphous nature of all the polymers and this can be attributed to the kinetically controlled polymerization reaction (Figure S7). It is well known that the combination of kinetic polymerization and propeller like conformation of TPE lead to the formation of amorphous 3D network of polymers. The field emission scanning electron microscopy (FESEM) images of **F$_x$CMPs** show the presence of spherical particles with an average size of 300-500 nm (Figure 1a-d and Figure S8). All the **F$_x$CMPs** have high thermal stability as observed by thermogravimetric analysis (TGA) (Figure S9). TGA of **F$_{0.0}$CMP** shows no appreciable weight loss till 350 °C, on further heating a continuous weight loss of nearly 50% is observed till 800 °C. On the contrary, **F$_{0.1}$CMP, F$_{0.5}$CMP** and **F$_{2.0}$CMP** show no significant weight loss upto 600 °C, however on further heating steady weight loss (10-20%) is observed. These results suggest that the incorporation of 9-fluorenone moiety into the polymeric network leads to an enhanced thermal stability of **F$_{0.1}$CMP, F$_{0.5}$CMP** and **F$_{2.0}$CMP**. Before studying permanent porosity, all the samples are activated at 150 °C under vacuum to remove any traces of guest solvent molecules. N$_2$ adsorption measurements of all **F$_x$CMPs** at 77 K show type-II profile, thereby suggesting non-porous nature with respect to N$_2$ (Figure 1e). CO$_2$ adsorption measurements at 195 K show the

Scheme 2. Synthetic scheme for the preparation of **F$_x$CMPs**

type-I profile with appreciable CO_2 uptake in the low pressure region, suggesting microporous (< 2 nm) nature of **FₓCMP**s (Figure 1f). At 1 bar pressure the amount of CO_2 uptake are 65, 109, 98 and 40 mL g^{-1} for **F$_{0.0}$CMP, F$_{0.1}$CMP**, **F$_{0.5}$CMP** and **F$_{2.0}$CMP**, respectively (Figure 1f). The decrease in the amount of N_2 (77 K) and CO_2 (195 K) uptake from **F$_{0.1}$CMP** to **F$_{2.0}$CMP** is attributed to the blockage of the pores by carbonyl functional group of the 9-fluorenone and also due to the higher degree entanglement with increasing concentration of 9-fluorenone-based connector. These results clearly suggest that it is possible to tune the pore size and surface area of the **FₓCMPs** by controlling the amount of 9-fluorenone within the polymer. Langmuir surface areas based on CO_2 desorption (195 K) are calculated to be 366 m^2/g, 612 m^2/g, 537 m^2/g and 226 m^2/g for **F$_{0.0}$CMP, F$_{0.1}$CMP, F$_{0.5}$CMP** and **F$_{2.0}$CMP**, respectively.

Tetraphenylethene (TPE) shows very weak or no emission in dilute solution due to the presence of non-radiative channels, induced by fast rotation of phenyl groups around C-C single bonds. However, TPE shows enhanced emission in solid state due to restricted phenyl rotation, induced by intermolecular Ph…Ph or C-H…Ph interactions (aggregation induced emission, AIE). The recent reports show that the enhanced emission of TPE can also be achieved by its integration into extended porous polymeric structure like CMP or metal-organic framework, either by strong covalent linkages or metal coordination, respectively.[7a],[13] Tetrakis(4-bromophenyl)ethene shows strong cyan emission (AIE) in solid state with maximum at 445 nm when excited at 380 nm (Figure S10 and S11). **F$_{0.0}$CMP** shows broad absorption in 250-450 nm range with maximum at 320 nm (Figure 2a). Corresponding emission spectrum of **F$_{0.0}$CMP** shows maximum at 520 nm (λ_{ex}= 380 nm) which is strongly red
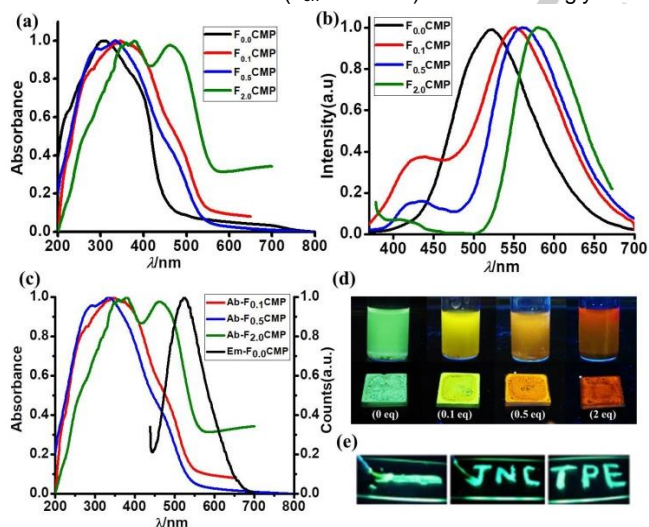

Figure 2. a) Absorption spectra and b) corresponding emission spectra of **F$_{0.0}$CMP** (black), **F$_{0.1}$CMP** (red), **F$_{0.5}$CMP** (blue), and **F$_{2.0}$CMP** (green), c) Spectral overlap of **F$_{0.1}$CMP**, **F$_{0.5}$CMP**, **F$_{2.0}$CMP** absorption and emission spectra of **F$_{0.0}$CMP**, d) Images of **F$_{0.0}$CMP**, **F$_{0.1}$CMP**, **F$_{0.5}$CMP**, and **F$_{2.0}$CMP** (from left to right) dispersed in THF (top) and drop casted on solid glass substrate (bottom) under UV light, e) Images of **F$_{0.0}$CMP** mixed with poly(ethylene glycol)-block-poly(propylene glycol)-block-poly(ethylene glycol) under UV light: Writing and coating.
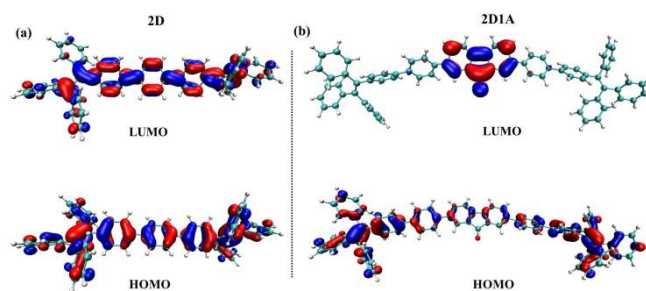

Figure 3. The frontier molecular orbitals (HOMO and LUMO) of a) **2D** and b) **2D1A** computed at the B3LYP/6-31G(d) level of theory.

shifted compared to tetrakis(4-bromophenyl)ethene emission (λ_{max} = 445 nm) (Figure 2b). Such red shifted emission occurs due to increased conjugation of TPE on polymerization with 1,4-diboronic acid and can be described as framework induced emission. **F$_{0.1}$CMP**, **F$_{0.5}$CMP** and **F$_{2.0}$CMP** also show broad absorption with maximum at 350 nm due to π-π^* transition of TPE and a new band is also observed at 480 nm (no such band is observed for **F$_{0.0}$CMP**) (Figure 2a). The intensity of this band enhances with increasing 9-fluorenone content from 0.1 to 2.0 eq (Figure 2a). The 470 nm absorption band is likely due to intramolecular charge transfer (ICT) from TPE to 9-fluorenone.[14] To interpret the experimental findings, we have carried out time-dependent density functional theory (TDDFT) calculations on simplified cluster models of **F$_{0.0}$CMP** and **F$_{2.0}$CMP**, which are denoted as **2D** and **2D1A**, respectively. The structure of **2D** comprises of two molecular units of TPE separated by a phenyl spacer. **2D1A** features two TPE and one 9-fluorenone units wherein the acceptor moiety is separated from the each TPE unit by a phenyl spacer. TDDFT results of **2D** reveal that the lowest energy excitation dominantly possesses π_{HOMO}-π^*_{LUMO} character and both frontier molecular orbitals (FMOs) are distributed throughout the entire length of the molecule (Figure 3a). On the contrary for **2D1A**, FMOs are found to be spatially separated. While the HOMO is concentrated on the TPEs, the LUMO localizes on the 9-fluorenone segment (Figure 3b). Consequently, the lowest energy excitation in **2D1A** possesses strong CT character which corresponds to ICT from the TPE units to the 9-fluorenone. The band gap of **F$_{0.0}$CMP**, **F$_{0.1}$CMP**, **F$_{0.5}$CMP** and **F$_{2.0}$CMP** are found to be 2.8, 2.5, 2.3 and 2.1 eV, respectively as calculated by Kubelka-Munk plots. These results suggest that band gap can be regulated by varying 9-fluorenone content in **FₓCMPs**. The photoluminescence spectra of **F$_{0.1}$CMP**, **F$_{0.5}$CMP** and **F$_{2.0}$CMP** (λ_{ex} = 350 nm), show two bands at 435, 430, 425 nm, assigned to the TPE component of the polymers and at 540, 560, 580 nm, assigned to the ICT emission of **F$_{0.1}$CMP**, **F$_{0.5}$CMP** and **F$_{2.0}$CMP**, respectively (Figure 2b). With increasing 9-fluorenone content, the lower wavelength emission band exhibits blue shift and decrease in intensity, while the ICT band is gradually red shifted (Figure 2b). ICT emission of **F$_{2.0}$CMP** at 580 nm is proved by recording solvent dependent emission spectra (Figure S12). In a nonpolar solvent, such as hexane the relative intensity of 580 nm band is weaker than 425 nm. With increasing solvent polarity

(CH_2Cl_2, CH_3CN and H_2O) the intensity of 580 nm band increases while the intensity of 425 nm decreases (Figure S12). The stabilization of 580 nm bands in polar solvent indicates the occurrence of ICT excited state, associated with TPE and 9-fluorenone.[7b] This is further supported by the excitation dependent emission spectra. When **F2.0CMP** is excited at 350 nm, a broad band at 580 nm is observed. On increasing the excitation wavelength from 350 to 450 nm, a gradual increase in the intensity of 580 nm band is observed (Figure S13). This indicates the intensity of 580 nm is higher when **F2.0CMP** is excited at CT absorption region rather than at lower wavelengths where contribution of TPE segment is higher. These results confirm the ICT emissions in **F0.1CMP**, **F0.5CMP** and **F2.0CMP**. It is interesting to note that, with increasing 9-fluorenone content the relative intensity of 425 nm band (λ_{ex}= 350 nm) in **F0.1CMP**, **F0.5CMP** and **F2.0CMP** which is assigned to the TPE segment, is quenched gradually (Figure 2b). Such quenching of TPE emission is surprising as it is the major component of **FxCMPs**, while only 0.1, 0.5 and 2 eq of 9-fluorenone are present in **F0.1CMP**, **F0.5CMP** and **F2.0CMP**, respectively. We also observe that the emission spectrum of **F0.0CMP** partially overlaps with the absorbance spectra of **F0.1CMP**, **F0.5CMP** and **F2.0CMP** (Figure 2c). Therefore, there is a chance of energy transfer from TPE segment to the ICT state. In order to support this, excitation spectra of **F0.1CMP**, **F0.5CMP** and **F2.0CMP** are recorded by monitoring the emission at 540, 560 and 580 nm, respectively (Figure S14). The excitation spectrum of **F2.0CMP** displays band corresponding to ICT at 470 nm and maxima at around 380 nm associated with TPE segment (Figure S14). This reveals the energy transfer from covalently bonded TPE segments (which are not involved in ICT) to TPE:9-fluorenone ICT state. Similar spectral features are observed in case of **F0.1CMP** and **F0.5CMP**. The excited state lifetime of **F2.0CMP**, monitored at 450 nm (this is the wavelength of TPE donor emission) is found to be negligible (0.7 ns) and shorter than pure TPE donor (1.9 ns), suggesting energy transfer from TPE to the TPE:9-fluorenone ICT state (Figure S15). Note, the lifetime of **F0.0CMP** monitored at λ= 480 nm was 1.36 ns. By exciting, **F2.0CMP** at λ= 373 and 480 nm and monitoring the emission at λ= 585 nm the excited state lifetime are measured to be 1.9 and 1.7 ns, respectively (Figure S16). Thus combining all the above results, it can be concluded that the charge transfer emissions of **F0.1CMP**, **F0.5CMP** and **F2.0CMP** are assisted by the energy transfer from TPE segments which are not involved in ICT, to the TPE:9-fluorenone ICT state. Both the energy transfer process and efficient charge transfer interactions in the polymer are responsible for tunable emission colour from green to red. In addition, the nanometer sized particles of **FxCMPs** result in highly processable dispersions in THF which are drop casted over large area substrates with no loss in emission intensity (Figure 2d). Also, the **FxCMPs** can be mixed with linear polymers, such as [poly(ethylene glycol)-block-poly(propylene glycol)-block-poly(ethylene glycol)] and are used for writing or coating applications (Figure 2e). The tunable band gap of **FxCMPs** (from 2.8 eV to 2.1 eV) inspired us to investigate the photocatalytic hydrogen evolution from water. In a typical experiment, 5 mg **FxCMPs** is dispersed in water/MeOH (3:1)
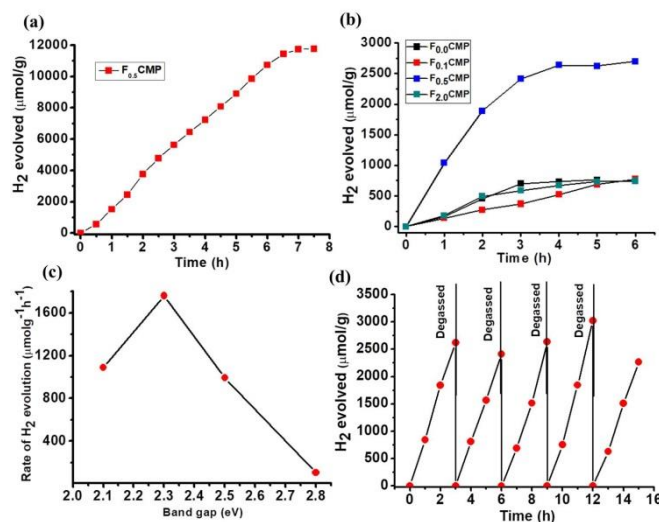

Figure 4. a) Time-course for photocatalytic H_2 production for **F0.5CMP** under broad-spectrum (λ>290 nm), b) Time-course for photocatalytic H_2 production for **F0.0CMP** (Black), **F0.1CMP** (red), **F0.5CMP** (blue), and **F2.0CMP** (green) using visible-light irradiation (λ>420 nm), c) Correlation of rate of H_2 evolution from **F0.0CMP**, **F0.1CMP**, **F0.5CMP**, and **F2.0CMP** using broad-spectrum irradiation with optical band gap, d) Cycling test of photocatalytic H_2 production for **F0.5CMP** under broad emission. The reaction mixture was degassed every 3 h (dashed line).

containing sodium sulfide/sodium sulfate as sacrificial hole-scavenger (Figure S17). The homogeneous dispersion is taken into an 80 ml photocatalytic reactor and purged with N_2 for 30 minutes to remove the dissolved oxygen. The system is irradiated (290 W Xenon arc lamp) under stirring condition to ensure uniform irradiation of the dispersion. MeOH was used to enhance the dispersability of **FxCMPs**. No additional noble metal co-catalyst was used in the reaction mixture to catalyze hydrogen evolution. The photocatalytic activity of the reaction mixtures are tested both under broad-spectrum (λ>290 nm) and visible light (λ>420 nm) irradiation. The time course of H_2 evolution is monitored by gas chromatography. All the **FxCMPs** show H_2 production under illumination with both broad-spectrum and visible light irradiation (Figure 4a, b and, Figure S18-S20). The **FxCMP** particles dispersed in aqueous solution absorbs photons and generate electrons and holes upon photo-irradiation. The photo-generated electrons reduce water to H_2, whereas the holes oxidize SH^- ions to H^+ and sulfur which eventually forms polysulfide and dissolve in water (Figure S29). Theoretical studies also indicate that the process is thermodynamically feasible. The rate of H_2 evolution under broad-irradiation is found to be 105.44, 992.61, 1759.92 and 1088.45 μmol g^{-1} h^{-1} for **F0.0CMP**, **F0.1CMP**, **F0.5CMP** and **F2.0CMP**, respectively (Figure S21). The rate of H_2 evolution increases gradually with decrease in optical band gap (Figure 4c). This is expected because the red-shift in optical band gap from **F0.0CMP** to **F0.5CMP** causes more absorption of photons and generation of more charge carriers which eventually facilitate the photocatalytic water splitting. However, **F2.0CMP** with lowest optical band gap (2.1 eV) shows a drastic drop in

Table 1. Photophysical properties and hydrogen evolution rates (HERs) for F_xCMPs.

CMPs	Optical band gap (eV)[a]	λ_{em} (nm)[b]	HER>420 nm ($\mu mol\ g^{-1}h^{-1}$)[c]	HER>290 nm ($\mu mol\ g^{-1}h^{-1}$)[c]
$F_{0.0}CMP$	2.8	530	183.66	105.44
$F_{0.1}CMP$	2.5	435. 540	129.21	992.61
$F_{0.5}CMP$	2.3	430, 560	659.55	1759.92
$F_{2.0}CMP$	2.1	425.580	124.23	1088.45

[a] Calculated from the absorption spectra of F_xCMPs, [b] Emission peaks of the F_xCMPs recorded in solid state, [c] Reaction condition: 5 mg F_xCMPs is dispersed in 40 ml water mixture containing sodium sulfide/sodium sulfate as sacrificial hole-scavenger and irradiated by 290 W Xe lamp for 6 h.

H_2 evolution rate, probably due to the non-radiative electron-hole recombination that becomes dominant after an optimum band gap.[14] Similar trend is observed when the same experiments are conducted using visible-light irradiation (Figure S22). The rate of H_2 evolution under visible-light irradiation is measured to be 183.66, 129.21, 659.55 and 124.23 $\mu mol\ g^{-1}\ h^{-1}$ for $F_{0.0}CMP$, $F_{0.1}CMP$, $F_{0.5}CMP$ and $F_{2.0}CMP$, respectively (Figure S23). Such lower visible light activity of F_xCMPs probably occurs due to less absorbance in the visible part of the absorption spectrum. Among all four CMPs, the highest photocatalytic activity is found in $F_{0.5}CMP$ (Table 1). Under broad-spectrum illumination a rate of 1759.92 $\mu mol\ g^{-1}\ h^{-1}$ is achieved which is 17 times higher than $F_{0.0}CMP$. More importantly, a significant improvement in visible light activity (659.55 $\mu mol\ g^{-1}\ h^{-1}$) is obtained and the value is comparable with the activities of recently reported polymers (Table S1). Here, we should mention that direct comparison between different reports is very difficult due to the variation in reaction setup/ conditions/ lamp power in different reports. The stability of $F_{0.5}CMP$ is studied by carrying out the "repeated runs" H_2 evolution experiment under broad-irradiation for total 15 hours. The reaction is stopped and the mixture is degassed after every 3 hours. As shown in Figure 4d, the photocatalytic performance of $F_{0.5}CMP$ is consistent and stable even after five consecutive cycles. Apparent quantum yield (AQY) of the photocatalytic H_2 evolution for $F_{0.5}CMP$ was found to be 5.8% with an excitation wavelength of 400nm. Interestingly, $F_{0.5}CMP$ does not show any significant changes in absorption, emission and FT-IR spectrum after 15 hours of irradiation ($\lambda> 290$ nm), indicating high stability and structural integrity (Figure S24- S26). To prove that irradiation of light plays the most important role in the H_2 evolution, we carry out the reaction under dark, maintaining the other reaction condition same. No H_2 evolution is detected even after 7 hours (Figure S27). A blank solution (without catalyst) containing sodium sulfide/sodium sulfate in water mixture is irradiated by broad-spectrum to ensure the effect of sacrificial agent in the total amount of hydrogen produced. No significant H_2 evolution is observed from the blank solution (Figure S28). These results confirm that evolution of hydrogen is occurred by reduction of proton via an electron

transfer process, and not simply by decomposition of F_xCMPs. Since F_xCMPs were synthesized by Pd-catalyzed Suzuki-Miyura cross coupling reaction, they are expected to contain certain amount of residual palladium. According to the previous literature reports, this residual palladium plays role in catalyzing hydrogen evolution.[15] The residual palladium contents of F_xCMPs, measured by ICP-OES and EDXS analysis were found to be insignificant. $F_{0.0}CMP$, $F_{0.1}CMP$, $F_{0.5}CMP$ and $F_{2.0}CMP$ contained 0.43, 0.39, 0.31 and 0.89 wt% of palladium, respectively (Table S2). Notably, the $F_{0.5}CMP$ which has lowest residual palladium content (0.31 wt% from ICP-OES) showed the highest rate of hydrogen evolution. At the same time, $F_{2.0}CMP$ having highest amount of residual palladium (0.89 wt% from ICP-OES) showed low rate of hydrogen evolution. Hence, there is no positive correlation between the residual palladium content and rate of hydrogen production. This indicates that residual palladium is not the major factor for the photocatalytic hydrogen evolution of F_xCMPs. Previously, Cooper and Yu *et al* also showed that there is no positive role of residual palladium content after the cross-coupling reaction in photocatalysis and our results are in consistence with their report.[4c-d], [15]

Conclusions

In conclusion, a new series of donor-acceptor conjugated microporous polymers containing TPE as donor and 9-fluorenone as acceptor have been synthesized and thoroughly characterized. The introduction of different amount of fluorenone acceptor segment in the polymer backbone resulted donor-acceptor polymers ($F_{0.1}CMP$, $F_{0.5}CMP$ and $F_{2.0}CMP$) with different band gaps and corresponding emission color. By controlling donor-acceptor ratio, the efficiency of energy transfer is tuned which resulted in tunable emission color ranging from green to red. All the donor-acceptor F_xCMPs exhibits excellent photocatalytic activity towards hydrogen generation and highest activity was found in $F_{0.5}CMP$s with 2.3 eV band gap. Our approach of using energy transfer and ICT for tuning the emission color and band gaps in CMPs would provide new strategies in fabricating highly efficient light emitting CMPs with no excitation energy annihilation which could be useful in light emitting diodes and photovoltaic. Also it will open a new path to rationally design efficient photocatalysts for water splitting towards hydrogen production.

Experimental Section

Synthesis of tetrakis(4-bromophenyl)ethene. Tetraphenylethene (0.77 mmol, 500 mg) was dissolved in dry dichloromethane (DCM) (20 mL) and cooled to 0 °C followed by addition of Br_2 (1.54 mmol, 0.04 mL). Reaction mixture was stirred at room temperature for 15 h, the excess Br_2 was quenched by adding aq. $Na_2S_2O_4$. Mixture was extracted with DCM and concentrated under reduced pressure. The crude product was purified by column chromatography by eluting with hexane. White solid, Yield: 80%.

Synthesis of 2, 7-biphenyl-9H-fluoren-9-one. 2, 7-dibromo-9H-fluoren-9-one (1.47 mmol, 500 mg) and phenylboronic acid (2.9 mmol, 361 mg)

were dissolved in dry THF (10 mL) and degassed/purged with N_2. To this, $Pd(PPh_3)_4$ (0.03 mmol, 33mg) was added followed by aq. K_2CO_3. The reaction mixture was refluxed for 24 h and cooled to room temperature. The mixture was added to water and extracted with DCM and filtered over Na_2SO_4. The solution was concentrated under reduced pressure to result in crystalline yellow solid. Yield, 60 %.

Synthesis of $F_{0.0}$CMP, $F_{0.1}$CMP, $F_{0.5}$CMP and $F_{2.0}$CMP. For synthesizing **$F_{0.0}$CMP**, a mixture of tetrakis(4-bromophenyl)ethene (0.15 mmol, 100 mg) and 1,4-benzenediboronic acid (0.3 mmol, 49 mg) were taken in a Schlenk tube and dissolved in dry DMF. The reaction mixture was allowed for freeze-thaw pump cycles and purged with N_2 continuously. $Pd(PPh_3)_4$ (0.0105 mmol, 12 mg) was added to the mixture under N_2 flow. After that aq. K_2CO_3 was added to the mixture and refluxed for 24 h under N_2 atmosphere. Precipitates were collected by filtration and washed with ethanol and THF for several times. Final purification was done using Soxhelet extraction with THF and methanol for 48 h each. EDAX: C, 96; Pd, 0.31. Similar reaction procedure was used for preparing **$F_{0.1}$CMP**, **$F_{0.5}$CMP** and **$F_{2.0}$CMP**, only difference was 0.1 eq (0.015 mmol), 0.5 eq (0.075 mmol) and 2.0 eq (0.3 mmol) of 2,7-dibromo-9H-fluoren-9-one was added, respectively in to the reaction mixture containing tetrakis(4-bromophenyl)ethene (0.15 mmol, 100 mg) and 1,4-benzenediboronic acid (0.3 mmol, 49 mg). In all cases, the product formed was purified using Soxhelet extraction with THF and methanol for 48 h.

Photocatalytic hydrogen evolution experiment. Photocatalytic H_2 evolution experiments were carried out in a 80 ml stoppered flask. 5 mg **F_xCMP** is dispersed in 40 ml water containing 0.75 M Na_2S and 0.75 M Na_2SO_4. The suspension was ultrasonicated to make a homogeneous dispersion which was later purged with N_2 for 30 minutes to remove all the dissolved gases. The reaction mixture was irradiated with 290 W Xe lamp (Newport) fitted with 12 cm path length of water filter for removal of IR radiation. A visible-bandpass filter (400 nm-800 nm) was used to block the UV-light. The evolved gas was analysed by Agilent CN15343150 Gas Chromatography which use a thermal conductivity detector referencing against a standard (H_2/N_2) gas mixture with a known concentration of hydrogen. No hydrogen evolution was observed for a mixture of water/methanol/0.75 M Na_2S and 0.75 M Na_2SO_4 under λ >290 nm irradiation in absence of a photocatalyst.

[1] a) S. Liu, Z. -R. Tang, Y. Sun, J. C. Colmenares, Y. –J. Xu, *Chem. Soc. Rev.,* **2015**, *44*, 5053-5075; b) M. G. Walter, E. L. Warren, J. R. McKone, S. W. Boettcher, Q. Mi, E. A. Santori, N. S. Lewis, *Chem. Rev.*, **2010**, *110*, 6446–6473; c) J. Nowotny, M. A. Alim, T. Bak, M. A. Idris, M. Ionescu, K. Prince, M. Z. Sahdan, K. Sopian, M. A. M. Teridi, W. Sigmund, *Chem. Soc. Rev.*, **2015**, *44*, 8424-8442.

[2] a) F. E. Osterloh, *Chem. Soc. Rev.,* **2013**, *42*, 2294-2320; b) J. Ran, J. Zhang, J. Yu, M. Jaroniec, S. Z. Qiao, *Chem. Soc. Rev.*, **2014**, *43*, 7787-7812; c) A. Kudo, Y. Miseki, *Chem. Soc. Rev.*, **2009**, *38*, 253-278; d) U. Maitra, B. S. Naidu, A. Govindaraj, C. N. R. Rao, *Proc. Natl. Acad. Sci. U.S.A.*, **2013**, *110*, 11704-11707; e) C. N. R. Rao, S. R. Lingampalli, *Small*, **2016**, *12*, 16-23; f) T. –D. Nguyen-Phan, S. Luo, Z. Li, A. D. Gamalski, J. Tao, W. Xu, E. A. Stach, D. E. Polyansky, S. D. Senanayake, E. Fujita, J. A. Rodriguez, *Chem. Mater.*, **2015**, *27*, 6282–6296; g) K. Maeda, K. Domen, *J. Phys. Chem. Lett.*, **2010**, *1*, 2655–2661; h) B. Banerjee, V. Amoli, A. Maurya, A. K. Sinha and A. Bhaumik, *Nanoscale.*, **2015**, *7*, 10504-10512; i) V. Amoli, M. Sibi, B. Banerjee, M. Anand, A. Maurya, S. Farooqui, A. Bhaumik, A. Sinha, *ACS Appl. Mater. Interfaces.* **2015**, *7*, 810-822. j) J. Qi, W. Zhang, R. Cao, *Adv. Energy Mater.* **2018**, *8*, 1701620; k) C. Gao, Q. Meng, K. Zhao, H. Yin, D. Wang, J. Guo, S. Zhao, L. Chang, M. He, Q. Li, H. Zhao, X. Huang, Y. Gao and Z. Tang, *Adv. Mater. (Weinheim, Ger.)* **2016**, *28*, 6485-6490; l) X. Ma, K. Zhao, H. Tang, Y. Chen, C. Lu, W. Liu, Y. Gao, H. Zhao, Z. Tang, *Small* **2014**, *10*, 4664-4670; m) H. Yin, S. Zhao, K. Zhao, A. Muqsit, H. Tang, L. Chang, H. Zhao, Y. Gao, Z. Tang, *Nat. Commun.* **2015**, *6*, 6430; n) W. Zhang, W. Lai, R. Cao, *Chem. Rev.* **2017**, *117*, 3717-3797.

[3] a) G. Zhang, Z. –A. Lan, X. Wang. *Angew. Chem. Int. Ed.* **2016**, *55*, 15712 – 15727; b) Mondal, S. K. Kundu, W. K. Hung Ng, R. Singuru, P. Borah, H. Hirao, Y. Zhao and A. Bhaumik, *Chem. Euro. J.*, **2015**, *21*, 19016-19027. c) A. M. Khattak, H. Sin, Z. A. Ghazi, X. He, B. Liang, N. A. Khan, H. R. Alanagh, A. Iqbal, L. Li, Z. Tang, *J. Mater. Chem. A* **2018**, *6*, 18827-18832; d) B. Liang, H. Wang, X. Shi, B. Shen, X. He, Z. A. Ghazi, N. A. Khan, H. Sin, A. M. Khattak, L. Li and Z. Tang, *Nat. Chem.* **2018**, *10*, 961-967.

[4] a) G. Mukherjee, J. Thote, H. B. Aiyappa, S. Kandambeth, S. Banerjee, K. Vanka, R. Banerjee, *Chem. Commun.*, **2017**, *53*, 4461-4464; b) R. S. Sprick, B. Bonillo, M. Sachs, R. Clowes, J. R. Durrant, D. J. Adams, A. I. Cooper, *Chem. Commun.*, **2016**, *52*, 10008—10011; c) R. S. Sprick, J. –X. Jiang, B. Bonillo, S. Ren, T. Ratvijitvech, P. Guiglion, M. A. Zwijnenburg, D. J. Adams, A. I. Cooper, *J. Am. Chem. Soc.* **2015**, *137*, 3265–3270; d) R. S. Sprick, B. Bonillo, R. Clowes, P. Guiglion, N. J. Brownbill, B. J. Slater, F. Blanc, M. A. Zwijnenburg, D. J. Adams, A. I. Cooper, *Angew. Chem.* **2016**, *128*, 1824 –1828; e) Y. Xu, N. Mao, S. Feng, C. Zhang, F. Wang, Y. Chen, J. Zeng, J. –X. Jiang, *Macromol. Chem. Phys.* **2017**, *218*, 1700049; f) S. Bandyopadhyay, A. G. Anil, A. James, A. Patra, *ACS Appl. Mater. Interfaces.* **2016** , *8*, 27669-27678; g)

[5] a) X. Wang, K. Maeda, A. Thomas, K. Takanabe, G. Xin, J. M. Carlsson, K. Domen, M. Antonietti, *Nat. Mater.*, **2009**, *8*, 76–80; b) X. Wang, S. Blechert, M. Antonietti, *ACS Catal.*, **2012**, *2*, 1596–1606; c) J. Liu, Y. Liu, N. Liu, Y. Han, X. Zhang, H. Huang, Y. Lifshitz, S.-T. Lee, J. Zhong, Z. Kang, *Science*, **2015**, *347*, 970–974; d) J. Bi, W. Fang, L. Li, J. Wang, S. Liang, Y. He, M. Liu, L. Wu, *Macromol. Rapid Commun.*, **2015**, *36*, 1799–1805; e) L. Stegbauer, K. Schwinghammer, B. V. Lotsch, *Chem. Sci.*, **2014**, *5*, 2789-2793; f) F. Haase, T. Banerjee, G. Savasci, C. Ochsenfeld, B. V. Lotsch, *Faraday Discuss.*, **2017**, *201*, 259-276; g) V. S. Vyas, F. Haase, L. Stegbauer, G. Savasci, F. Podjaski, C. Ochsenfeld, B. V. Lotsch, *Nat. Commun.*, **2015**, *6*, 8508; h) T. Banerjee, F. Haase, G. Savasci, K. Gottschling, C. Ochsenfeld, B. V. Lotsch, *J. Am. Chem. Soc.*, **2017**, *139*, 16228–16234.

[6] a) Y. Xu, S. Jin, H. Xu, A. Nagai, D. Jiang, *Chem. Soc. Rev.*, **2013**, *42*, 8012-8031; b) N. Chaoui, M. Trunk, R. Dawson, J. Schmidt, A. Thomas, *Chem. Soc. Rev.*, **2017**, *46*, 3302-3321; c) Y.-B. Zhou, Z.-P. Zhan, *Chem. Asian. J.*, **2018**, *13*, 9; c) R. Dawson, A. Laybourn, R. Clowes, Y. Z. Khimyak, D. J. Adams, A. I. Cooper, *Macromolecules.*, **2009**, *42*, 8809–8816; d) P. Lindemann, M. Tsotsalas, S. Shishatskiy, V. Abetz, P. Krolla-Sidenstein, C. Azucena, L. Monnereau, A. Beyer, A. Gölzhäuser, V. Mugnaini, H. Gliemann, S. Bräse, C. Wöll, *Chem. Mater.*, **2014**, *26*, 7189–7193; e) B. Kiskan, J. Weber, *ACS Macro Lett.*, **2012**, *1*, 37–40; f) A. I. Cooper, *Adv. Mater.*, **2009**, *21*, 1291–1295; f) S. Bandyopadhyay,

S. Kundu, A. Giria, A. Patra, *Chem. Commun.*, **2018**, *54*, 9123-9126; g) S. Bandyopadhyay, C. Singh, P. Jash, M. W. Hussain, A. Paul, A. Patra, *Chem. Commun.*, **2018**, *54*, 6796-6799.

[7]   a) V. M. Suresh, S. Bonakala, S. Roy, S. Balasubramanian, T. K. Maji, *J. Phys. Chem. C.*, **2014**, *118*, 24369-24376; b) V. M. Suresh, A. Bandyopadhyay, S. Roy, S. K. Pati, T. K. Maji, *Chem. Eur. J.*, **2015**, *21*, 10799-10804; c) A. Li, H. –X. Sun, D. –Z. Tan, W. –J. Fan, S. –H. Wen, X. –J. Qing, G. –X. Li, S. –Y. Li, W. –Q. Deng, *Energy Environ. Sci.*, **2011**, *4*, 2062-2065; d) X. Liu, Y. Xu, D. Jiang, *J. Am. Chem. Soc.*, **2012**, *134*, 8738–8741; e) J. –X. Jiang, F. Su, A. Trewin, C. D. Wood, H. Niu, J. T. A. Jones, Y. Z. Khimyak, A. I. Cooper, *J. Am. Chem. Soc.*, **2008**, *130*, 7710–7720; f) L. Chen, Y. Honsho, S. Seki, D. Jiang, *J. Am. Chem. Soc.*, **2010**, *132*, 6742–6748.

[8]   a) T. Hisatomi, J. Kubota, K. Domen, *Chem. Soc. Rev.*, **2014**, *43*, 7520-7535; b) C. Wang, K. E. deKrafft, W. Lin, *J. Am. Chem. Soc.*, **2012**, *134*, 7211–7214; c) W. J. Youngblood, S. –H. A. Lee, K. Maeda, T. E. Mallouk, *Acc. Chem. Res.*, **2009**, *42*, 1966–1973; d) A. W. Peters, Z. Li, O. K. Farha, J. T. Hupp, *ACS Appl. Mater. Interfaces.,* **2016**, *8*, 20675−20681; e) X. Sun, Q. Yu, F. Zhang, J. Wei, P. Yang, *Catal. Sci. Technol.*, **2016**, *6*, 3840–3844; f) E. Depontia, M. Natali, *Dalton Trans.*, **2016**, *45*, 9136–9147; g) J. –D. Xiao, Q. Shang, Y. Xiong, Q. Zhang, Y. Luo, S. –H. Yu, H. -L. Jiang, *Angew. Chem. Int. Ed.*, **2016**, *55*, 9389 – 9393.

[9]   a) N. J. Hestand, R. V. Kazantsev, A. S. Weingarten, L. C. Palmer, S. I. Stupp, F. C. Spano, *J. Am. Chem. Soc.* **2016**, *138*, 11762−11774; b) A. S. Weingarten, R. V. Kazantsev, L. C. Palmer, D. J. Fairfield, A. R. Koltonow, S. I. Stupp, *J. Am. Chem. Soc.*, **2015**, *137*, 15241−15246; c) H.-W. Li, Z. Guan, Y. Cheng, T. Lui, Q. Yang, C.-S. Lee, S. Chen, S.-W. Tsang, *Adv. Electron. Mater.*, **2016**, *2*, 1600200.

[10]   a) R. S. Kularatne, H. D. Magurudeniya, P. Sista, M. C. Biewer, M. C. Stefan, *J. Polym. Sci. A Polym. Chem.*, **2013**, *51*, 743-768; b) J. –S. Wu, S. –W. Cheng, Y. –J. Cheng, C. –S. Hsu, *Chem. Soc. Rev.*, **2015**, *44*, 1113-1154; c) T. Marszalek, M. Lia, W. Pisula, *Chem. Commun.*, **2016**, *52*, 10938-10947; d) M. Gao, J. Subbiah, P. B. Geraghty, M. Chen, B. Purushothaman, X. Chen, T. Qin, D. Vak, F. H. Scholes, S. E. Watkins, M. Skidmore, G. J. Wilson, A. B. Holmes, D. J. Jones, W. W. H. Wong, *Chem. Mater.*, **2016**, *28*, 3481–3487; e) M. He, W. Li, Y. Gao, H. Tian, J. Zhang, H. Tong, D. Yan, Y. Geng, F. Wang, *Macromolecules.*, **2016**, *49*, 825–832.

[11]   a) V. G. Pavelyev, O. D. Parashchuk, M. Krompiec, T. V. Orekhova, I. F. Perepichka, P. H. M. van Loosdrecht, D. Y. Paraschuk, M. S. Pshenichnikov, *J. Phys. Chem. C*, **2014**, *118*, 30291–30301; b) K. Kailasam, M. B. Mesch, L. Möhlmann, M. Baar, S. Blechert, M. Schwarze, M. Schröder, R. Schomäcker, J. Senker, A. Thomas, *Energy Technol.* **2016**, *4*, 744; c) Y. Xu, N. Mao, C. Zhang, X. Wang, J. Zeng, Y. Chen, F. Wang and J.-X. Jiang, *Appl. Catal. B: Environ.*, **2018**, *228*, 1-9; d) Z. Wang, X. Yang, T. Yang, Y. Zhao, F. Wang, Y. Chen, J. H. Zeng, C. Yan, F. Huang and J.-X. Jiang, *ACS Catal.*, **2018**, *8*, 8590-8596; e) D. Schwarz, A. Acharja, A. Ichangi, P. Lyu, M. V. Opanasenko, F. R. Goßler, T. A. F. König, J. Čejka, P. Nachtigall, A. Thomas, M. J. Bojdys, *Chem. Eur. J.* **2018**, 24, 11916; f) X.-H. Zhang, X.-P. Wang, J. Xiao, S.-Y. Wang, D.-K. Huang, X. Ding, Y.-G. Xiang and H. Chen, *J. Catal.*, **2017**, *350*, 64-71.

[12]   L. Li, W. Lo, Z. Cai, N. Zhang, L. Yu, *Macromolecules*, **2016**, *49*, 6903–6909.

[13]   N. B. Shustova, B. D. McCarthy, M. Dinca, *J. Am. Chem. Soc.,* **2011**, *133*, 20126-20129.

[14]   A. P. Kulkarni, X. Kong, S. A. Jenekhe, *Macromolecules.*, **2006**, *39*, 8699.

[15]   L. Li, Z. Cai, Q. Wu, W.-Y. Lo, N. Zhang, L. X. Chen, L. Yu, *J. Am. Chem. Soc.,* **2016**, 138, 7681−7686.

FULL PAPER

Entry for the Table of Contents

FULL PAPER

A series of donor-acceptor CMPs with tunable band gap, showing energy transfer assisted charge transfer emission is exploited as efficient photocatalysts for hydrogen evolution.
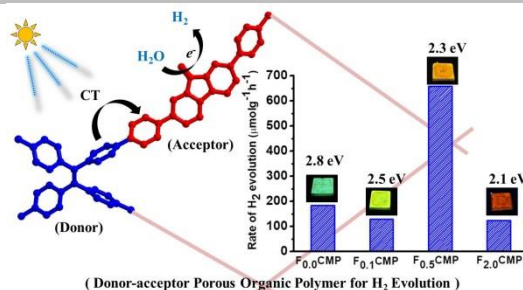
(Donor-acceptor Porous Organic Polymer for H₂ Evolution)

Venkata Suresh Mothika [a],#, Papri Sutar[a],#, Parul Verma[a], Shubhajit Das[b], Swapan K Pati[b] and Tapas Kumar Maji[a],*

Title: Regulating charge-transfer in conjugated microporous polymer for photocatalytic hydrogen evolution